

Proof-of-principle experiment for nanoparticle-assisted laser wakefield acceleration

Constantin Aniculaesei^{1,*}, Vishwa Bandhu Pathak¹, Kyung Hwan Oh¹, Calin Ioan Hojbota^{1,3}, Prashant Kumar Singh¹, Bo Ram Lee¹, Hyung Taek Kim^{1,2}, Enrico Brunetti⁴, Byung Ju Yoo¹, Jae Hee Sung^{1,2}, Seong Ku Lee^{1,2}, Chang Hee Nam^{1,3}

¹Center for Relativistic Laser Science, Institute for Basic Science (IBS), Gwangju 61005, Republic of Korea.

²Advanced Photonics Research Institute, Gwangju Institute of Science and Technology (GIST), Gwangju 61005, Republic of Korea

³Department of Physics and Photon Science, GIST, Gwangju 61005, Republic of Korea.

⁴Scottish Universities Physics Alliance, University of Strathclyde, Department of Physics, Glasgow, G4 0NG, United Kingdom.

*email: ca182@ibs.re.kr

In the present work, we demonstrate for the first time a proof-of-principle experiment for nanoparticle-assisted laser wakefield acceleration. The nanoparticles, generated through laser ablation of aluminium, were introduced into the plasma and used to trigger the injection of electrons into the nonlinear plasma wake excited by a high power femtosecond laser. In this experiment, a significant enhancement of the electron beam energy, energy spread and divergence is obtained compared with the case when electrons are self-injected. The best quality electron bunches presented peak energy up to 338 MeV with a relative energy spread of 4.7% and vertical divergence of 5.9 mrad. This method can be further improved by adding an aerodynamic lens system, for instance, which would control the nanoparticle size, density, material and injection position thus allowing accurate control of the laser wakefield accelerator.

INTRODUCTION

A laser wakefield accelerator¹ (LWFA) uses the plasma waves generated from the interaction between a high power laser and a plasma to accelerate electrons to relativistic energies. In the highly nonlinear case of laser-plasma interaction called “bubble”² or “blowout”³ regime, the laser pulse pushes the plasma electrons forward and sideways leaving behind a spherical region filled with ions. The displaced electrons form a sheath around the bubble and oscillate around the laser propagation axis with a frequency equals to the plasma frequency. Some of the electrons that collide at the base of the bubble can be injected into the bubble in a process called wave-breaking^{4,5}. The condition for electron self-injection is that the electrons group velocity is greater than the phase velocity of the back of the bubble⁶. The electron injection carries on until the space-charge effect of the injected electrons is strong enough to stop further injection. Due to the highly nonlinear evolution of the plasma waves, the onset of self-injection depends on the initial conditions of the laser pulse and plasma medium thus leading to some degree of randomness in the self-injection process, consequently affecting the parameters of the accelerated electron bunch. To overcome the randomness of the injection process various schemes have been developed to manipulate the longitudinal momentum of the electrons surrounding the plasma wake^{7,8} or the phase velocity of the plasma wake^{9,10}.

In 2007 a new laser wakefield acceleration scheme was proposed by Shen et al.¹¹ and further theoretically investigated in 2018 by Cho et al.¹² with multi-dimensional particle-in-cell (PIC) simulations. This new electron acceleration scheme uses a nanowire or a nanoparticle to trigger the injection of the electrons in the acceleration phase of the plasma wakes. In these studies, it was assumed that the nanoparticle/nanowire is fully ionized by the leading edge of the laser pulse, creating a strong electric field that attracts some of the plasma electrons, which can gain additional momentum and be injected into the bubble. These theoretical studies predicted that the parameters

of the accelerated beam depend on the nanoparticle composition, size or number and also on the moment/position when the nanoparticle is injected into the bubble. Assuming full ionization, the composition or the size of the nanoparticle controls the number of electrons injected in the wake, and therefore the charge of the accelerated bunch. The number of nanoparticles controls the number of electron bunches injected into the wake thus controlling the bunch length, structure and total charge. Injecting the electrons at earlier or later times leads to accurate control of the electron beam energy by increasing the acceleration length and ensuring that the injection can happen when the strength of the accelerating field of the wake is the highest. Thus, the nanoparticle-assisted wakefield acceleration (NA-LWFA) could be a versatile scheme due to its high degree of control over the wakefield acceleration process.

Since this kind of scheme was first proposed more than 12 years ago, there have been, to the author's best knowledge, no experimental attempts to test the viability of NA-LWFA. For best performance, the NA-LWFA scheme would require¹² an aerodynamic lens system¹³ (ALS) that delivers a stream of nanoparticles that can be injected, ideally one nanoparticle at the time, into the plasma wake with micrometre precision. An ALS is not only bulky and expensive but also requires a serious engineering effort to integrate it with a gas target. We decided to investigate first the feasibility of a simplified NA-LWFA scheme that does not employ an ALS device. This work, if successful, would give the motivation to invest time and effort in developing an NA-LWFA with ALS. As a source of nanoparticles, we used laser ablation¹⁴ and we integrated it with a supersonic gas jet. This alternative scheme lacks the possibility of controlling the position where the nanoparticle is injected in the plasma wake, but the nanoparticle size and number can be controlled¹⁵ by tuning the fluence of the laser beam used for ablating material. The nanoparticle + helium gas mixture then supersonically expands in a vacuum chamber, interacting with a high power femtosecond laser and generating an electron beam. In the present case, the ablation laser fluence is reduced until the density of nanoparticles is, theoretically, low enough to assume that the main laser interacts with only a few nanoparticles. The reduction of the laser fluence has been done while monitoring the electron beam parameters as shown in Methods. The results obtained from this proof-of-principle NA-LWFA experiment are presented in the next section followed by a brief discussion regarding some aspects of the electrons injection in the plasma wake in the presence of a nanoparticle.

RESULTS

The setup used for NA-LWFA is described in Methods. The accelerated electron beam has been characterized in terms of vertical and horizontal divergence, peak energy and relative energy spread. The peak energy is defined as the electron energy where the spectrum presents the highest charge density. For all the shots the gas nozzle inlet helium pressure has been set at 10.5 bar, corresponding to a measured plasma density of $5 \times 10^{18} \text{ cm}^{-3}$ at a distance of 1.5 mm above the nozzle. The main laser was focused at the beginning of the gas jet density ramp and fixed at 1.5 mm above the nozzle. These settings have been chosen after a systematic scanning of the experimental parameters until the most stable electron beam has been obtained with helium gas. When used, the ablation laser arrives 10 microseconds before the main pulse, a delay empirically set after systematic scanning until the best quality electron beam has been obtained with nanoparticle-assisted electron injection.

We recorded two data sets: with and without nanoparticles present in the helium gas jet. From each dataset, we selected for the present work the best 10 shots, as displayed in Figure 1 and Figure 2. A summary of the results is shown in Table 1. In the case of LWFA with electron self-injection, the quality of the electron beam is very poor, with relative energy spread (shown in Figure 1a and Table 1) larger than 30% and divergence (shown in Figure 2a and Table 1) larger than 12 mrad. A significant enhancement in electron beam quality has been observed when nanoparticles triggered the electron injection. In this case, the relative energy spread (shown in Figure 1b and Table 1) is as small as 4.5% while the divergence (shown in Figure 2b and Table 1) decreases to 6 mrad. Most of the shots recorded with nanoparticles shared the same specific signature: low divergence, electron bunches very well defined spatially and in energy, with a very low energy spread and higher peak energy. A small number of the shots (about 10% of the total number of 74 shots) had very poor quality, which could be due to the lack of interaction of the main laser pulse with the nanoparticle. Since the number of nanoparticles is, according to theoretical calculations (see Methods), very small it is possible that some shots missed the nanoparticles.

It is interesting to observe that for the shots shown in the present work the peak electron energy recorded with nanoparticles presents a systematic higher electron energy than the electron energy obtained with self-injection. This result could be due two reasons: space charge effects and acceleration length. As shown in Table 1 the relative charge of the electron bunches generated from NA-LWFA is much smaller than the charge of the electron bunches recorded with self-injection. The charge of the bunch modifies locally the acceleration field of the plasma wake thus higher charge means smaller effective acceleration field. The acceleration length is the distance over which the electrons are accelerated. From three-dimensional PIC simulations (not shown here) using the real experimental parameters we observed that the electron injection into the plasma wake happens almost at the end of the gas jet. In contrast, in the case of NA-LWFA the electron injection can happen as soon as the plasma wake encounters an ionized nanoparticle. Since the nanoparticles are assumed uniformly distributed in the volume of the gas jet it is very probable that the nanoparticle-triggered electron injection could happen at much earlier times than the self-injection leading to a much longer acceleration length.

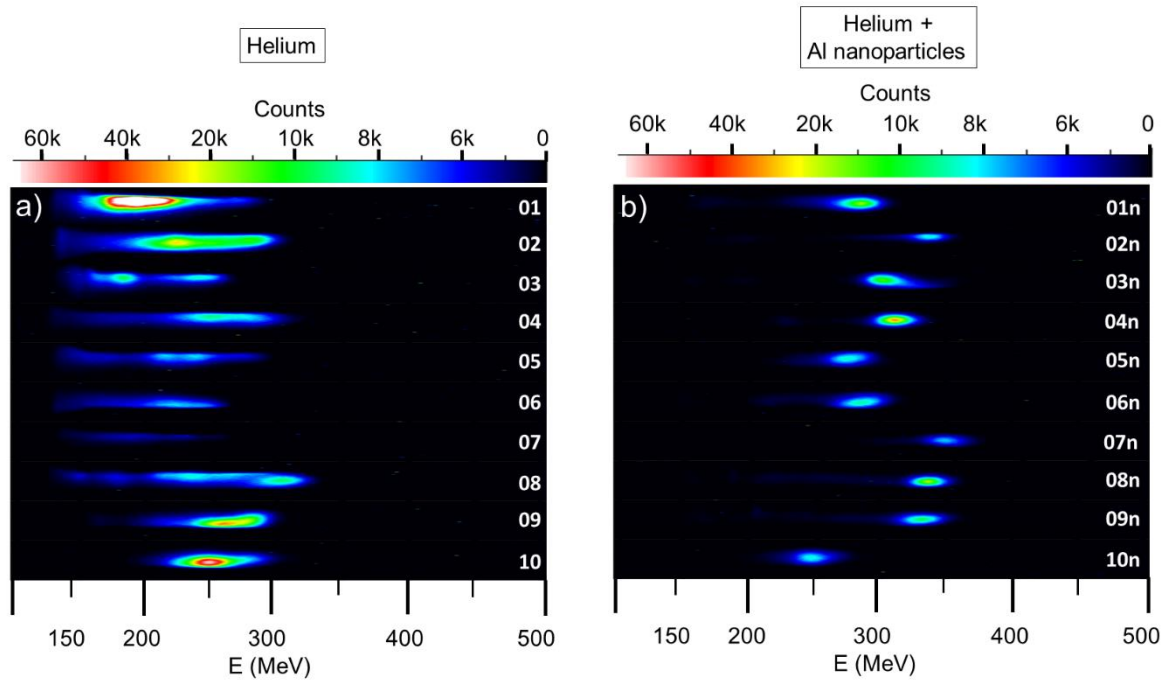


Figure 1 False-color images of the electron energy spectrum recorded in the electron spectrometer. a) shows some of the best electron spectra generated without assistance from nanoparticles and b) shows some the best energy spectra of the electrons generated with nanoparticles. When nanoparticles are used to control the electron injection in the “bubble” the electron energy spread is significantly reduced compared with the case when the electron injection is uncontrolled (when only helium is used).

No shot	RMS Peak energy (MeV)	RMS Relative energy spread (%)	RMS Horizontal divergence (mrad)	RMS Vertical divergence (mrad)	Relative Charge (a.u)
01	187	31.5	22.1	9.3	29.2
02	139	71.9	26.1	12.5	21.1
03	215	141.8	13.2	16.0	25.6
04	174	27.5	27.2	18.4	42.5
05	247	64.7	20.6	23.1	23.4
06	182	64.2	23.9	12.3	8.3
07	192	60.9	11.7	7.2	18.5
08	178	37.6	17.2	12.3	20.0
09	235	77.4	19.1	11.0	4.6
10	202	49.5	18.2	31.8	7.8
01n	275	9.0	12.1	9.3	1.6
02n	338	4.7	8.1	5.7	0.6
03n	306	6.4	6.9	7.0	1.3
04n	312	5.4	5.3	4.1	0.7
05n	276	8.2	8.2	6.9	0.8
06n	286	7.9	6.2	6.1	1.2
07n	344	5.5	5.8	6.4	0.3
08n	338	4.5	7.1	5.9	0.9
09n	331	6.0	20.0	6.4	0.8
10n	248	8.9	23.3	16.1	1.1

Table 1: Summarized electron beam parameters for the selected shots. The shot number with suffix “n” corresponds to the data taken in the presence of nanoparticles.

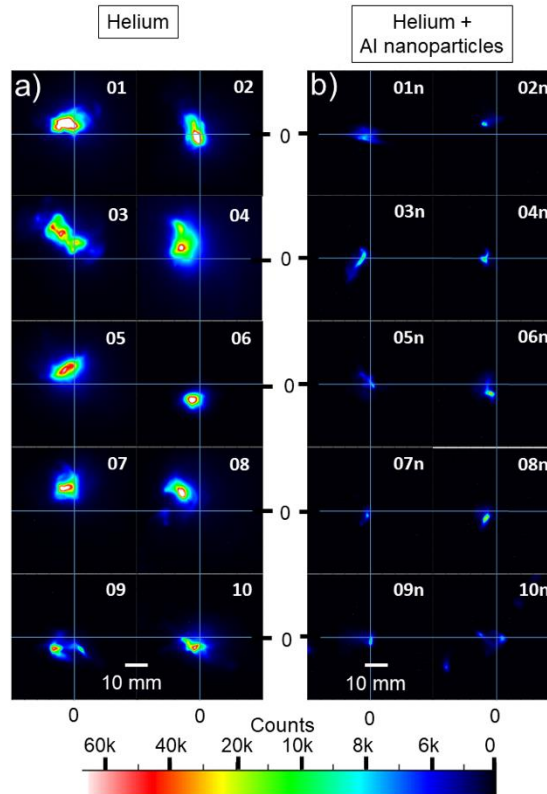


Figure 2 False-color images of the electron beam transverse distribution recorded by Lanex 1. a) shows the electron beam profiles obtained without nanoparticles and b) shows the electron beam profiles obtained with nanoparticles. When nanoparticles are used the electron beam divergence is reduced compared with the case when the electron injection is uncontrolled.

DISCUSSION

To get an insight into the process of electron injection via nanoparticle-assisted wakefield acceleration^{11,12} we run two-dimensional particle-in-cell (PIC) simulations using OSIRIS¹⁶. Details about the simulations can be found in Methods. Figure 3 shows the time evolution of the plasma density (a1 to f1) and longitudinal phase space (a2 to f2) to clarify the role of nanoparticles in the injection. As the laser propagates through the pre-ionized plasma, it pushes background plasma electrons (BPE) away from the axis, exciting a non-linear space-charge field, also referred as wakefield, just behind the laser due to the immobile ions (Figure 3 a1). When the laser encounters a pre-ionized and charge-neutral nanoparticle, it pushes the nanoparticle electrons (NPE) away from the axis, and excites a localized space-charge field which grows stronger as the rising-intensity part of the laser pulse passes through it (Figures a2-c2), and imparts extra momentum to the electrons in the vicinity of the laser pulse (Figure c2). As the nanoparticle approaches the falling-intensity region, due to reducing ponderomotive force, the BPE, as well as some fraction on NPE which were trapped in the front part of the laser, are trapped in the nanoparticle potential, and as the nanoparticle passes through the nonlinear wakefield, these electrons do the same as well (Figure d2). As the nanoparticle approaches the back of the wakefield (Figure e2), the effective field around the nanoparticle again changes in the presence of the strong plasma sheath created by the crossing of BPE. This results in the release of nanoparticle trapped electrons into the wakefield (Figure e2 and

f2). As the nanoparticle passes through the laser (Figures b1-f1), it also triggers transverse plasma modulations¹¹ in the electrons in the front part of the laser. Since these electrons, due to snow-ploughing effect¹⁷, stay in the front part of the laser on longer time scales, the transverse modulations as well stay with the laser, at the same time extending to the whole wakefield region and evolving transversely.

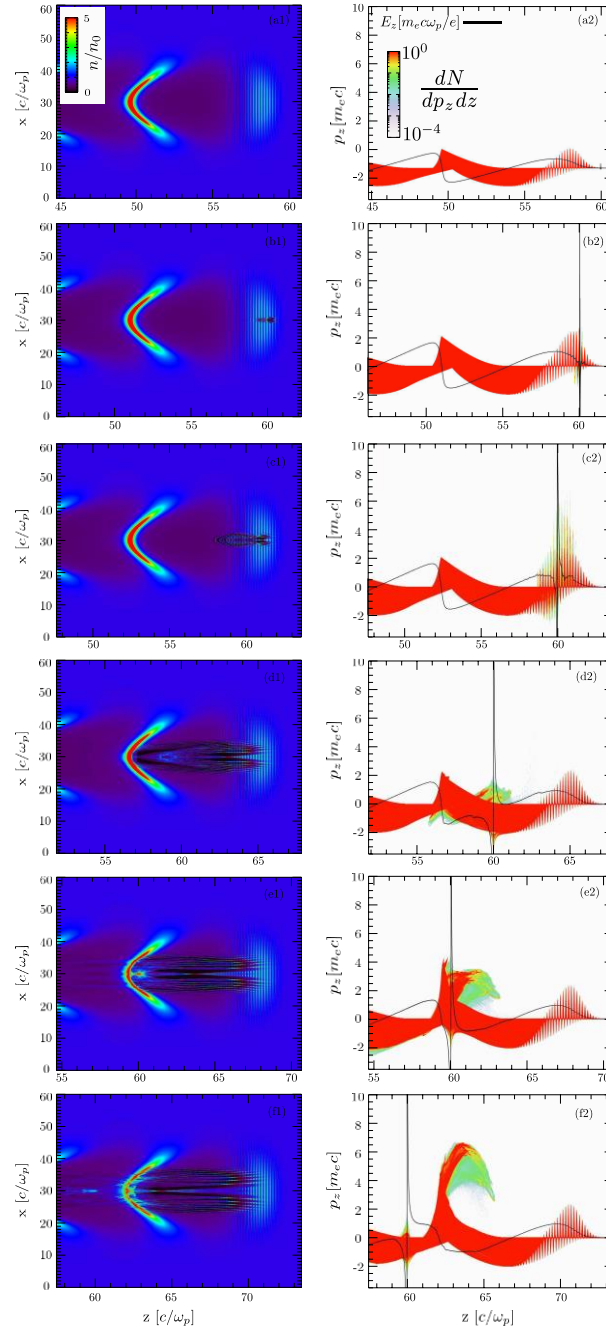


Figure 3: 2D PIC simulations highlighting the nanoparticle-assisted trapping of plasma electrons in the non-linear wakefield excited by the laser. Snapshots of plasma density profiles at progressing times are shown in (a1) - (e1), and corresponding phase-space diagrams are shown in (a2)-(e2). The solid lines in (a2)-(e2) are the on-axis longitudinal fields, and the spike in the fields are due to the nanoparticle space charge. A fully-ionized nanoparticle is initialized at $z = 60c/\omega_p$, and the window is moving with velocity c following the laser pulse.

These modulations in the density profile in the laser vicinity can strongly diffract the laser. This may

explain why in experiments, in presence of nanoparticles, no self-injection is observed. It is also worth mentioning here that in our simulations we do not observe any injection caused by these transverse density modulations as predicted by Shen et al.¹¹

Although we have shown in the present work a comparison between results obtained with self-injection scheme and nanoparticle-assisted injection scheme, we want to emphasize that we do not claim that self-injection always generates poor quality electron beams. Results from other works show that it is possible¹⁸⁻²¹ to obtain, using the self-injection scheme, a fairly good quality electron beam, although the exact laser parameters which lead to a good quality electron beam are not yet identified.

In this experiment, self-injection was very hard to achieve and, overall, the accelerated electron beam based on self-injection has shown a very poor quality. During the experiment, we measured strong nanosecond laser pre-pulses of the order of 10^{-4} relative to the main pulse, thus we can assume that the energy in the main pulse is much lower than what we measured using the full beam. The presence of the pre-pulse could also lead to coulomb explosion of the nanoparticle¹¹ but, if present, it did not seem to affect the quality of the most of the electron bunches. Even in these conditions, where the laser energy could be close or lower than required for the self-injection scheme, the nanoparticle-assisted electron injection managed to enhance significantly the electron beam quality. This result has been predicted theoretically¹¹ and could have important consequences in the development of kHz femtosecond laser wakefield accelerators²². In such accelerators, due to present technology constraints, the laser energy is currently limited to a few 10's of mJ thus requiring high-density, small-length gas targets to produce an electron beam. Using nanoparticles to assist the electron injection into the plasma wakes would help to produce a much better electron beam quality than currently achieved thus opening the road towards developing applications for the kHz, mJ laser wakefield accelerators.

This proof-of-principle experiment of NA-LWFA can be further improved using the same setup presented in this work but with a more stable laser. This should solve the shot to shot stability of the electron beam thus permitting a systematic scan of more experimental conditions such as the use of femtosecond ablation laser or different ablated materials.

Since the NA-LWFA has been proved in the present work to be a viable scheme, the time, effort and expense would be justified in order to further integrate an ALS with a gas target. This would allow control the charge of the accelerated electron beam, energy and energy spread.

From our 2D PIC simulations we observed that the bunch length, at the end of the acceleration process, is of the order of 1 micrometer (or less than 3.3 femtoseconds long). This results suggests that attoseconds long bunches could be produced if the number of electrons injected can be controlled. 3D PIC simulations could reveal the exact conditions in which shorter electron bunches could be produced using NA-LWFA scheme and, if proved to be realizable experimentally, could open new ways to applications such as generation of ultrashort sources of radiation²³⁻²⁵.

MATERIALS AND METHODS

The gas + nanoparticles target system

The gas jet + nanoparticles target consisted of two main parts: the supersonic nozzle and the source of nanoparticles. The supersonic nozzle was a conical *de Laval* type of nozzle with 2 mm inlet diameter, 3.9 mm outlet diameter and 8° semi-opening angle. The helium gas was fed into the nozzle through a 2 mm diameter pipe placed sideways (see Figure 3). The gas target was mounted on a motorized stage that controlled the movement of the nozzle in all three spatial directions. To limit the amount of gas released in the chamber during the experiment, the gas was fed through a solenoid valve (Parker Series 9) and operated in pulsed mode with an opening time of 6 ms; the laser pulse interacted with the gas jet 3 ms after valve opening.

The bottom part of the nozzle is a removable 2 mm thick aluminium plate fixed with screws. The nanoparticle source is based on laser ablation. The ablation laser (AL) with a wavelength of 532 nm, 3 ns pulse length and a diameter of 5 mm is focused down into the gas nozzle and ablates the surface of the removable plate. Previously published results have shown that the ablation plume produced by a nanosecond, picosecond or femtosecond laser can contain significant amounts of nanoparticles and micron-sized structures. The density and size of nanoparticles generated through laser ablation depend on the laser fluence, laser pulse length and the type of material ablated. The ablation plume mixes with the gas and is transported towards the outlet of the nozzle where it interacts with the main laser beam. The energy of the AL has been empirically set to 10 mJ per pulse, for which the divergence and energy spread of the electron beam was the lowest. In these conditions, the AL fluence on the target was 10.39 J/cm², which, according to published works, creates nanoparticles with sizes of the order of 10's of nm. This assumption has been confirmed by Atomic Force Microscopy measurements (not shown here) which showed that the majority of the generated nanoparticles had diameters between 10 nm and 20 nm. Optical probing using the interferometry could not show any phase shift when interferograms with and without nanoparticle present have been compared, which means that the nanoparticle density is much lower than the sensitivity of the interferometer. Using a theoretical estimation based on the amount of ablated material¹⁵ and assuming that all the material is transformed into spherical nanoparticles with 20 nm diameter we obtain a number of nanoparticles of the order of 10⁸ nanoparticles per shot. This estimation is based on idealized parameters, thus the number of nanoparticles is expected to be much lower. Changing the time delay between the ablation laser and the main laser and monitoring the quality of the accelerated electron beam it was easy to observe that the nanoparticles influence can be seen for approximately 3 microseconds. Taking into account the gas jet speed, which was supersonic (1400 m/s), we can estimate that the nanoparticles were present in a cylindrical volume with 4 mm diameter and 4.2 mm height. The density of nanoparticles can be approximated then to be between 10⁷-10⁸ nanoparticles/cm³.

The laser wakefield accelerator

The experiment has been run at Center for Relativistic Laser Science (CoReLS), Institute for Basic Science (IBS), South Korea and the setup is shown in Figure 3.

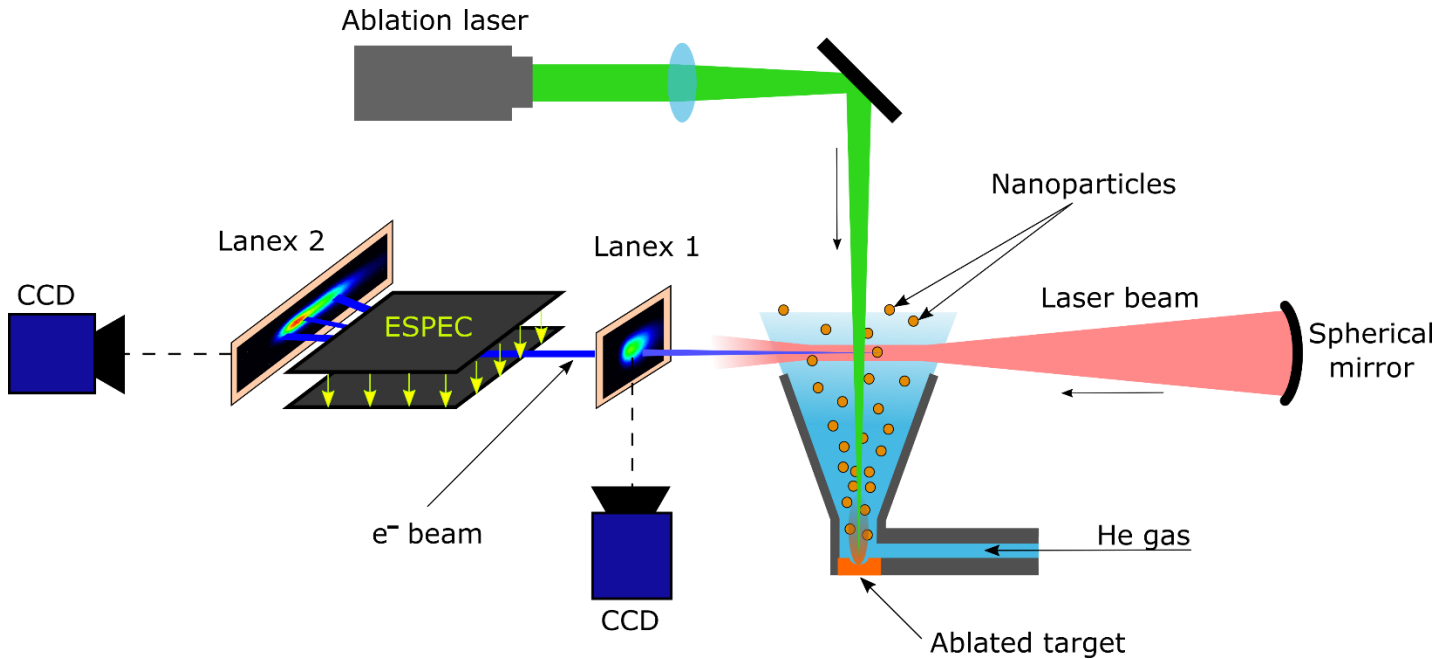


Figure 3: The setup used in the nanoparticle-assisted laser wakefield acceleration. The nanoparticles generated through laser ablation mix with He gas and co-propagate towards the outlet region where the high power laser excites nonlinear Langmuir plasma waves in the bubble or blowout regime. The accelerated electron bunches are diagnosed using Lanex1 (transverse profile, pointing, divergence and charge) and Espec+Lanex2 (energy and energy spread).

The setup was installed in a vacuum chamber maintained, before opening the gas valve, at a pressure of 10^{-5} mbar and consisted of a high power laser, focusing optics, gas nozzle and electron beam diagnostics. The Ti:Sapphire high power laser, with a central wavelength of 800 nm and horizontal polarization, is based on the chirped pulse amplification technique²⁶ and delivered 1.8 J pulses (after compressor) with a temporal duration of 27 ± 2 femtoseconds at a frequency of 5 Hz. A spherical mirror with the focal length of 1 meter focused down the 65 mm diameter laser beam to a focal spot with a diameter of 40 microns measured at full-width-at-half-maximum (FWHM), which contained 60% of the total energy. This ensured on target a normalized FWHM vector potential $a_0 = 1.07$.

For the entire experiment the laser beam was focused at the start of the density ramp, 1.5 mm longitudinally from the centre of the nozzle, with the spot placed horizontally in the centre of the gas nozzle and vertically at a distance of 1.5 mm from the nozzle exit. The transverse and longitudinal alignment was done with a Top View imaging setup which consists of a CCD camera (FLIR BFLY-U3-50H5M-C) equipped with a camera lens (Samyang 135 mm F2.8 ED UMC) and a BG39 glass filter to cut the scattered light from the laser. The Top View setup was also used to monitor the optical emission from the plasma channel due to nonlinear Thomson scattering^{27,28} and other plasma emission processes.

LanexTM 1 setup consisted of a 6x6 cm Gd₂O₂S:Tb screen (LanexTM Back) placed at 410 mm from the gas jet and imaged onto a CCD camera (FLIR BFLY-U3-50H5M-C) with a camera lens (Samyang 100 mm F2.8 ED UMC) and provides information about the transverse electron profile,

pointing, divergence and relative charge. The results for each dataset (taken in the same experimental conditions) were averaged and the mean value and the mean standard error was calculated.

The electron spectrometer (E-spec) consisted of a 0.996 T dipole magnet that has an opening with a height, width and length of 8×70×205 mm. The entrance of the E-spec was placed at a distance of 455 mm from the gas nozzle and dispersed the electrons in the horizontal direction as a function of their energy onto a 430×80 mm Gd₂O₂S:Tb screen (Lanex™ Back) placed at 1155 mm from the gas nozzle. The Lanex™ screen was imaged onto a CCD camera (FLIR GS3-U3-50S5M-C) with a lens (Samyang 16 mm F1.4 AS UMC). The error in energy reading of the electron spectrometer was determined by the electron beam size and pointing and varied depending on energy between (+6, -3.2) MeV for 175 MeV and (+35, -15.7) MeV for 400 MeV. The energy calibration of the electron spectrometer was done using the G4beamline code²⁹.

After energy calibration, the peak energy (the part of the energy spectrum that contains most of the charge) was determined by finding the maximum of counts from the image and reading the corresponding energy.

Particle-in-cell simulation

We performed a set of 2D PIC simulations using OSIRIS¹⁶ in order to illustrate the physics behind the nano-particle assisted trapping of electrons in the non-linear wakefield. A two-dimensional, moving with velocity c , simulation box (x - z) is considered with dimensions $20 \times 60 (c/\omega_p)^2$ divided into 20000×60000 cells. We consider a preformed neutral plasma of two species: plasma electrons, initialized with 4×4 particle per cell, and nanoparticle electrons, initialized with 100×100 particles per cell. For the simulation we consider a laser with $a_0 = 3.0$, FWHM spot diameter $D_0 = 40\mu m$, and FWHM pulse length $\tau_0 = 30 fs$, is propagating in pre-ionized plasma with density $5 \times 10^{18} cm^{-3}$. A pre-ionized, 20 nm in diameter and $100n_{cr}$ in charge density, nano size plasma is initialized on laser axis.

We could not run three dimensional (3D) PIC simulations due to the high grid resolution required to resolve the nanoparticle in 3D PIC simulation which made the computational cost prohibitive for us. Also, one can notice the higher a_0 used in the 2D simulations as compared to the experiments. This is done purposefully to match position of self-injection (without nanoparticle) in 2D simulations with the full scale 3D simulations taking into account the laser parameters same as used in the experiments, *ie.*, $a_0 = 1.0$, FWHM spot diameter $D_0 = 40\mu m$, and FWHM pulse length $\tau_0 = 30 fs$. We observe that in both the cases the self-injection occurs around plasma length of 5mm.

For the 3D (2D) simulations, without the nanoparticle, we consider a moving box, propagating with velocity c , of dimensions $20 \times 60 \times 60 (c/\omega_p)^3$ ($20 \times 60 (c/\omega_p)^2$) divided into $2000 \times 600 \times 600$ (2000×600) cells, and 2 (16) particles per cell for the BPE.

Acknowledgements

The authors thank the OSIRIS consortium at UCLA and IST for providing access to OSIRIS 3.0 framework.

This work has been supported by the Institute for Basic Science of Korea under IBS-R012-D1.

H.T.K., J.H.S., and S.K.L also supported by GIST through “Research on Advanced Optical Science

and Technology” grant in 2017.

E.B. acknowledges funding from U.K. EPSRC (EP/J018171/1, EP/N028694/1)

Competing interests:

The authors declare that they have no competing interests.

Contributions

C.A conceived the idea, designed the setup including the nozzle + nanoparticle source, participated in the experiment, run data analysis, interpreted the results and wrote the manuscript, V.B.P interpreted the data through PIC simulations, K.H.O, C.I.H, P.K.S and B.R.L assisted the organization of the experiment, E.B wrote the code used for data acquisition and processing, J.H.S and S.K.L supported the laser maintenance, H.T.K was the team leader, C.H.N is the Director of CoReLS. All the authors reviewed the manuscript.

Bibliography:

1. Tajima, T. & Dawson, J. M. Laser Electron Accelerator. *Phys. Rev. Lett.* **43**, 267–270 (1979).
2. Pukhov, A. & Meyer-ter-Vehn, J. Laser wake field acceleration: The highly non-linear broken-wave regime. *Appl. Phys. B Lasers Opt.* **74**, 355–361 (2002).
3. Lu, W., Huang, C., Zhou, M., Mori, W. B. & Katsouleas, T. Nonlinear theory for relativistic plasma wakefields in the blowout regime. *Phys. Rev. Lett.* **96**, 165002 (2006).
4. Modena, A. *et al.* Electron acceleration from the breaking of relativistic plasma waves. *Nature* **377**, 606–608 (1995).
5. Zhao, Z. *et al.* Nonlinear theory for relativistic plasma wakefields in the blowout regime. *Phys. Rev. Lett.* **10**, 1–4 (2006).
6. Esarey, E., Schroeder, C. B. & Leemans, W. P. Physics of laser-driven plasma-based electron accelerators. *Rev. Mod. Phys.* **81**, 1229–1285 (2009).
7. Faure, J. *et al.* Controlled injection and acceleration of electrons in plasma wakefields by colliding laser pulses. *Nature* (2006). doi:10.1038/nature05393
8. Kotaki, H., Masuda, S., Kando, M., Koga, J. K. & Nakajima, K. Head-on injection of a high quality electron beam by the interaction of two laser pulses. *Phys. Plasmas* (2004). doi:10.1063/1.1751171
9. Schmid, K. *et al.* Density-transition based electron injector for laser driven wakefield accelerators. *Phys. Rev. Spec. Top. - Accel. Beams* (2010). doi:10.1103/PhysRevSTAB.13.091301
10. Suk, H., Barov, N., Rosenzweig, J. B. & Esarey, E. Plasma electron trapping and acceleration in a plasma wake field using a density transition. *Phys. Rev. Lett.* (2001). doi:10.1103/PhysRevLett.86.1011
11. Shen, B. *et al.* Electron injection by a nanowire in the bubble regime. *Phys. Plasmas* (2007). doi:10.1063/1.2728773
12. Cho, M. H., Pathak, V. B., Kim, H. T. & Nam, C. H. Controlled electron injection facilitated by nanoparticles for laser wakefield acceleration. *Sci. Rep.* (2018). doi:10.1038/s41598-018-34998-0
13. Liu, P., Ziemann, P. J., Kittelson, D. B. & McMurry, P. H. Generating Particle Beams of Controlled Dimensions and Divergence .2. Experimental Evaluation of Particle Motion in Aerodynamic Lenses and Nozzle Expansions. *Aerosol Sci. Technol.* (1995). doi:10.1080/02786829408959749
14. Kim, M., Osone, S., Kim, T., Higashi, H. & Seto, T. Synthesis of nanoparticles by laser ablation: A review. *KONA Powder and Particle Journal* (2017). doi:10.14356/kona.2017009
15. Leitz, K. H., Redlingshöer, B., Reg, Y., Otto, A. & Schmidt, M. Metal ablation with short and ultrashort laser pulses. in *Physics Procedia* (2011). doi:10.1016/j.phpro.2011.03.128
16. Fonseca, R. A. *et al.* OSIRIS: A Three-Dimensional, Fully Relativistic Particle in Cell Code for Modeling Plasma Based Accelerators. in *International Conference on Computational Science* (2002).
17. Decker, C. D., Mori, W. B., Tzeng, K. C. & Katsouleas, T. The evolution of ultra-intense, short-pulse lasers in underdense plasmas. *Phys. Plasmas* (1996). doi:10.1063/1.872001
18. Brunetti, E. *et al.* Low Emittance, High Brilliance Relativistic Electron Beams from a Laser-Plasma Accelerator. *Phys. Rev. Lett.* **105**, 215007 (2010).
19. Banerjee, S. *et al.* Generation of tunable, 100-800 MeV quasi-monoenergetic electron beams from a laser-wakefield accelerator in the blowout regime. *Phys. Plasmas* **19**, 056703 (2012).
20. Wang, X. *et al.* Quasi-monoenergetic laser-plasma acceleration of electrons to 2 GeV. *Nat. Commun.* **4**, 1988 (2013).
21. Wiggins, S. M. *et al.* High quality electron beams from a laser wakefield accelerator. *Plasma Phys. Control. Fusion* (2010). doi:10.1088/0741-

22. Gustas, D. *et al.* High-charge relativistic electron bunches from a kHz laser-plasma accelerator. *Phys. Rev. Accel. Beams* (2018). doi:10.1103/PhysRevAccelBeams.21.013401
23. Albert, F. & Thomas, A. G. R. Applications of laser wakefield accelerator-based light sources. *Plasma Phys. Control. Fusion* **58**, 103001 (2016).
24. Schlenvoigt, H. P. *et al.* A compact synchrotron radiation source driven by a laser-plasma wakefield accelerator. *Nat. Phys.* **4**, 130–133 (2008).
25. Jaroszynski, D. A. *et al.* Radiation sources based on laser-plasma interactions. *Philos. Trans. R. Soc. A Math. Phys. Eng. Sci.* (2006). doi:10.1098/rsta.2005.1732
26. Strickland, D. & Mourou, G. Compression of amplified chirped optical pulses. *Opt. Commun.* **56**, 219–221 (1985).
27. Esarey, E., Ride, S. K. & Sprangle, P. Nonlinear Thomson scattering of intense laser pulses from beams and plasmas. *Phys. Rev. E* **48**, 3003–3021 (1993).
28. Chen, S. Y., Maksimchuk, A. & Umstadter, D. Experimental observation of relativistic nonlinear Thomson scattering. *Nature* **396**, 653–655 (1998).
29. Roberts, T. J. & Kaplan, D. M. G4beamline simulation program for matter-dominated beamlines. in *Proceedings of the IEEE Particle Accelerator Conference* 3468–3470 (2007). doi:10.1109/PAC.2007.4440461